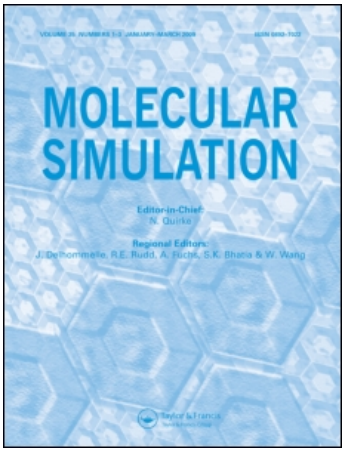

Molecular Simulation
Publication details, including instructions for authors and subscription information:
http://www.informaworld.com/smpp/title~content=t713644482

Thermal and pressure-induced martensitic phase transformations in a Ni-Al alloy modelled by Sutton-Chen embedded atom method

S. Kazanc[a]; S. Ozgen[a]
[a] Department of Physics, Faculty of Arts and Sciences, Firat University, Elazig, Turkey

To cite this Article Kazanc, S. and Ozgen, S.(2008) 'Thermal and pressure-induced martensitic phase transformations in a Ni-Al alloy modelled by Sutton-Chen embedded atom method', Molecular Simulation, 34: 3, 251 — 257
To link to this Article: DOI: 10.1080/08927020701742323
URL: http://dx.doi.org/10.1080/08927020701742323

Molecular Simulation
Vol. 34, No. 3, March 2008, 251–257

Taylor & Francis
Taylor & Francis Group

Thermal and pressure-induced martensitic phase transformations in a Ni–Al alloy modelled by Sutton–Chen embedded atom method

S. Kazanc* and S. Ozgen

Department of Physics, Faculty of Arts and Sciences, Firat University, Elazig, Turkey

(*Received 27 June 2007; final version received 10 October 2007*)

The Ni–Al alloys which exhibit the thermoelastic martensitic phase transformations in the composition range from 60 to 65 atomic percentage (at.%) of Ni are widely used in the high technology applications. In this study, both thermal and pressure-induced phase transformations in Ni-37.5 at.%Al alloy model were investigated by a molecular dynamics (MD) method. Physical interactions between atoms in the alloy system were modelled using the Sutton–Chen version of the embedded atom method based on many-body interactions. The potential parameters for cross interactions between Ni and Al atoms were estimated by optimising the results obtained from the MD simulations, taking into account the experimental data including the crystal lattice properties of the model alloy in high temperature phase.

Keywords: thermoelastic phase transformation; embedded atom method; molecular dynamics simulation; Ni–Al alloy

1. Introduction

Martensitic phase transformations which occur thermoelastically in most of the materials, such as Ni–Al, Cu–Ni and Ni–Ti alloys, are first-order solid–solid phase transformations and take place with collective motion of atoms [1,2]. These transformations can progress with changes in temperature and/or externally applied stress [3].

The Ni–Al alloys are attractive as possible high-temperature structural materials because of their high melting temperatures, low densities, high thermal conductivities and excellent oxidation resistance [4,5]. At the Ni-rich side of the Ni–Al phase diagram, several ordered phases are known to be exist. The ordered B2 structure of CsCl type prototype, a high temperature phase of the alloys called β-phase, is stable at high temperatures over a wide composition range of 40–68 at.%Ni. Above 63 at.%Ni, the B2 phase undergoes a martensitic transformation upon quenching to the tetragonal $L1_0$ ordered structure [6]. Also, the alloy has a super elasticity behaviour when deformed at above the martensite start temperature (M_s). It is well known that the pseudoelastic behaviour is related to the austenite–martensite phase transformations that occur thermoelastically [7]. Thermally and pressure-induced martensitic transformations have a thermoelastic character, controlled by the reduction in Gibbs' free energy of the system. This free energy consists of the chemical free energy and the mechanical potential energy, which depend on the temperature and the applied pressure, respectively. In fact, at the suitable temperature region, the applied pressure on the austenite phase increases the ratio of transformed martensite body [8]. Although many experimental studies have been reported on these transformations in macroscopic level, theoretical or experimental studies in atomic scale are very limited and difficult because of the anharmonic effects. However, molecular dynamics (MD) simulations allow us to study the structural changes during the transformation from austenite to martensite phase, or the reverse transition.

MD method computes the phase space trajectory of each atom in an array, according to Newton mechanics, so the evolution of the model system from an initial state to a final state at desired temperature and/or pressure can be determined [9]. Hence, MD simulations allow us to study the structural changes during the transformation from austenite to martensite phase, or the reverse transition. However, the choice of the potential energy functions and the determination of its parameters are the main factors on the validity of the results from MD simulations.

Recently, the martensitic transformations have been investigated in FeNi [10], B2 NiAl [3,11,12], TiV BCC alloys [13], B2 TiNi [14] and NiAl nanowires [15,16] using various types of empirical and semi-empirical potential functions in MD simulations. If the pairwise interatomic interactions are used instead of the potential energy functions including the density-dependent term in MD simulations, some properties of metals such as elastic constants and phonon spectra are not correctly calculated. The pairwise interatomic interactions can be used to determine qualitatively the above-mentioned properties of metals, but these interactions cannot warrant quantitatively the consistency with the experimental data.

*Corresponding author. Email: skazanc@firat.edu.tr

ISSN 0892-7022 print/ISSN 1029-0435 online

DOI: 10.1080/08927020701742323
http://www.informaworld.com

Daw and Baskes have proposed an alternative method to the pair potential approach based on the many-body idea, called the embedded atom method (EAM). However, due to the simplicity of their potential functions, the versions of the EAM proposed by Vother–Chen [17], Finnis–Sinclair [18] and Sutton–Chen [19] are widely used in the investigations of metallic systems and its alloys. The determination of the potential parameters, especially for the cross potential functions in alloy systems, is still a problem, although different approximations have been used to estimate their values [20,21].

In this study, to model the physical interactions among the atoms of Ni-37.5 at.%Al alloy, the Sutton–Chen version of the EAM (SCEAM) was used. The parameters of the potential energy functions for the model alloy were taken as given in literature for monatomic interactions, but the parameters for the cross interactions between Ni and Al atoms were calculated from the mixing rule of Lorentz–Berthelet because these parameters were not found in literature. However, for the calculated cross potential parameters, the stable model system of B2 type super-cell cannot be observed in MD simulations at high temperatures. So, another way to determine the cross interactions parameters was necessary. Therefore, the cross potential parameters were optimised by using MD simulations, taking into account the lattice properties of the alloy system at high temperature phase. Hence, we obtained the stable model system in B2 structure at high temperatures and investigated the martensitic transformations that occurred in our model system based on the SCEAM with the optimised parameters.

2. The simulation procedure

The MD method which allows the system to vary in shape and size, proposed by Parrinello and Rahman [22], was used for the investigation of the martensitic phase transformations occurring both thermally and pressure-induced, in Ni-37.5 at.%Al alloy selected as the model system. The Lagrangian function in Parrinello–Rahman theory is given by [3,23,24];

$$\mathcal{L}_{\mathrm{PR}}(\mathbf{r}^N, \dot{\mathbf{r}}^N, \mathbf{h}, \dot{\mathbf{h}}) = \frac{1}{2}\sum_{i=1}^{N} m_i\left(\dot{\mathbf{s}}_i^t \mathbf{G}\dot{\mathbf{s}}_i\right) - \sum_{i=1}^{N}\sum_{j>i}^{N}\phi(|\mathbf{h}\mathbf{s}_{ij}|) + \frac{1}{2}M\mathrm{Tr}(\dot{\mathbf{h}}^t\dot{\mathbf{h}}) - P_{\mathrm{ext}}V \tag{1}$$

where N is the number of particle, m_i is the mass of particle i, $\mathbf{s}_i$ is a column vector which has elements changing between zero. The lengths of the MD cell axis are described with three vectors $\mathbf{A}(t)$, $\mathbf{B}(t)$ and $\mathbf{C}(t)$ as a function of time. Furthermore, components of the Cartesian coordinates of these vectors constitute a matrix $\mathbf{h} = (\mathbf{A}, \mathbf{B}, \mathbf{C})$ which defines the volume of the MD cell, $V = \det(\mathbf{h})$. The metric tensor $\mathbf{G}$ is given by matrix product $\mathbf{h}^t\mathbf{h}$, M is an arbitrary constant which has mass in unit and P_{ext} is external pressure applied on the cell. Thus, the square of distance between particles i and j is described by $r_{ij}^2 = \mathbf{s}_{ij}^t\mathbf{G}\mathbf{s}_{ij}$. The classical equations of motion of the system are obtained from the potential energy function,

$$\ddot{\mathbf{s}}_i = -\frac{1}{m_i}\mathbf{F}_i - \mathbf{G}^{-1}\dot{\mathbf{G}}\dot{\mathbf{s}}_i \tag{2}$$

$$\ddot{\mathbf{h}} = M^{-1}(\Pi - \mathbf{I}P_{\mathrm{ext}})\sigma \tag{3}$$

where $\sigma = (\mathbf{B}\times\mathbf{C}, \mathbf{C}\times\mathbf{A}, \mathbf{A}\times\mathbf{B}) = V(\mathbf{h}^{\mathrm{t}})^{-1}$ and microscopic stress tensor, Π, is a dyadic given as follows;

$$\Pi = V^{-1}\left[\sum_{i=1}^{N} m_i v_i v_i - \sum_{i=1}^{N}\sum_{j>i}^{N}\frac{F_{ij}}{r_{ij}}\mathbf{r}_{ij}\mathbf{r}_{ij}\right] \tag{4}$$

In a binary alloy of type-a and type-b atoms, the total energy of a crystal with N atoms in the SCEAM methodology is given by;

$$\begin{aligned} E_T^{\mathrm{SC}} = &\left\{\frac{1}{2}\sum_{i^{\mathrm{a}},j^{\mathrm{a}}}^{N^{\mathrm{a}}}\varepsilon_{\mathrm{a}}\left(\frac{A_{\mathrm{a}}}{r_{ij}}\right)^{n_{\mathrm{a}}} - \sum_{i^{\mathrm{a}}}^{N^{\mathrm{a}}}\varepsilon_{\mathrm{a}}c_{\mathrm{a}}\left[\sum_j\left(\frac{A_{\mathrm{a}}}{r_{ij}}\right)^{m_{\mathrm{a}}}\right]^{1/2}\right\} \\ &+\left\{\frac{1}{2}\sum_{i^{\mathrm{b}},j^{\mathrm{b}}}^{N^{\mathrm{b}}}\varepsilon_{\mathrm{b}}\left(\frac{A_{\mathrm{b}}}{r_{ij}}\right)^{n_{\mathrm{b}}} - \sum_{i^{\mathrm{b}}}^{N^{\mathrm{b}}}\varepsilon_{\mathrm{b}}c_{\mathrm{b}}\left[\sum_j\left(\frac{A_{\mathrm{b}}}{r_{ij}}\right)^{m_{\mathrm{b}}}\right]^{1/2}\right\} \\ &+\frac{1}{2}\sum_{i^{\mathrm{a}},j^{\mathrm{b}}}^{N^{\mathrm{ab}}}\varepsilon_{\mathrm{ab}}\left(\frac{A_{\mathrm{ab}}}{r_{ij}}\right)^{n_{\mathrm{ab}}} + \frac{1}{2}\sum_{i^{\mathrm{b}},j^{\mathrm{a}}}^{N^{\mathrm{ba}}}\varepsilon_{\mathrm{ba}}\left(\frac{A_{\mathrm{ba}}}{r_{ij}}\right)^{n_{\mathrm{ba}}} \end{aligned} \tag{5}$$

where, i^{a} and i^{b} indicating summation over type-a and type-b atoms, respectively. The potential parameters for different types of atoms in an alloy system can be calculated from Lorentz–Berthelet [20],

$$A_{\mathrm{ab}} = A_{\mathrm{ba}} = \frac{A_{\mathrm{a}} + A_{\mathrm{b}}}{2}, \quad n_{\mathrm{ab}} = n_{\mathrm{ba}} = \frac{n_{\mathrm{a}} + n_{\mathrm{b}}}{2}, \quad m_{\mathrm{ab}} = m_{\mathrm{ba}} = \frac{m_{\mathrm{a}} + m_{\mathrm{b}}}{2} \tag{6}$$

$$\varepsilon_{\mathrm{ab}} = \varepsilon_{\mathrm{ba}} = \sqrt{\varepsilon_{\mathrm{a}}\varepsilon_{\mathrm{b}}}. \tag{7}$$

The values of parameters for Ni and Al elements are given in Table 1. By using the parameters obtained from equations (6) and (7) for the cross interactions, we could not observe the stable model system with B2 type super-cell. Therefore, only the potential parameter $\varepsilon_{\mathrm{NiAl}}$ was optimised by means of MD simulations. The optimisation process was carried out by adjusting the cross parameter $\varepsilon_{\mathrm{NiAl}}$ so that the model system will be stable in the high temperature phase and has a lattice parameter which is in

Table 1. The parameters of Sutton–Chen version of the EAM functions [20].

Matter	ε ($\times 10^{-2}$eV)	A(Å)	c	m	n
Ni	1.5707	3.52	39.432	6	9
Al	3.3147	4.05	16.399	6	7

agreement with experimental one, using bisection method. Hence, the best estimated value of the cross parameter ε_{NiAl} is 0.0201 eV.

The structural analysis was done by using the atomic positions, besides the radial distribution functions $g(r)$ (RDF) and the mean square displacements $\langle R^2 \rangle$ (MSD), calculated respectively as [8,9];

$$g(r) = \frac{V}{N^2} \left\langle \frac{\sum_{i=1}^{N} n_i(r)}{4\pi r^2 \Delta r} \right\rangle. \tag{8}$$

Here, r is the radial distance, $n_i(r)$ is the coordination number of atom i separated with r within Δr interval, and bracket denotes the time average [9],

$$\langle R^2 \rangle = \frac{1}{N} \sum_{i=1}^{N} [\mathbf{r}_i(t) - \mathbf{r}_i(0)]^2. \tag{9}$$

In our study, the simulations were performed on three dimensional arrays of 10 × 10 × 10 unit cells (2000 atoms). The ideal B2 superlattice structure of Ni-37.5 at.%Al model alloy was chosen as the starting configuration for the MD simulations. The initial velocities were derived from a random number generator so as to confirm a Maxwell–Boltzmann distribution at a given temperature initially. In the MD cell, 1000 Ni and 750 Al atoms were located at the corners and centres of the unit super-cells respectively and the extra 250 Ni occupying atoms were randomly assigned on the Al sublattice sites. To avoid the effects of free surfaces in the simulated array, periodic boundary conditions were acted on three directions of the MD cell. The potential functions were truncated at a cut-off distance of 2.5 times the equilibrium lattice constant of the alloy. The temperature of the model system was controlled by rescaling the atomic velocities at every two integration steps. The equation of motion was numerically solved by using the Gears' five order predictor–corrector algorithm with integration step size of 5.5 fs.

3. Results and discussion

3.1 Thermally induced transformation

To investigate the thermally induced solid–solid phase transformations in the Ni-37.5 at.%Al alloy, the equilibrated model system in the structure of B2 type super-cell at 700 K was cooled to 350 K at intervals of 50 K (Figure 1(a)). The MD simulations at each temperature run for 20,000 integration steps. As seen from Figure 1(a) and 1(b), when the system temperature is decreased to 400 K, the changes in some quantities such as the cohesive energy (E), MSD ($\langle R^2 \rangle$), the lengths (a, b, c) and angles (α, β, γ) of the MD cell axis, which is an important indicator to show how the MD cell is deformed [25], are observed. The deviation in the MSD during the transformation from β-phase to product phase was calculated as 0.05 Å^2 (Figure 1(b)). Because the deviation in the MSD is smaller than the distance between atoms, it can be said that the transformation exhibits a diffusionless behaviour which is a typical character observed experimentally for thermoelastic phase transformations [26]. It can be seen from Figure 1(a) that the value of MD cell axis in three axes kept almost the same until the temperature reached 400 K, which means the B2 structure (austenite) is stable when the temperature is higher than 400 K. But after the transformation there is a change on the MD cell axis, which indicates that the MD simulation box underwent a distortion. The reason for this distortion is that faults occurred by slipping of atomic planes, twinning, stacking faults in the structure, which are also observed experimentally [26]. Afterwards, in order to observe the reverse transformation the temperature of the system was raised to 700 K with the same ratio of cooling process. When the temperature reached a value of 550 K during the heating process, the changes in the structural quantities occurred again because the martensite structure became unstable, and simultaneously the transformation from martensite to austenite started. From these observations, one can say that the martensite structure of the model system transforms reversibly to austenite phase.

The RDF curves obtained at every temperature set during cooling and heating cycle between 700 and 350 K are shown in Figure 2. The model alloy has a B2 super-cell (with bcc unit cell) in the austenite phase at 700 K. The first peak location on the RDF curve denotes the nearest interatomic distances and was estimated as 2.53 Å at 700 K in our study. The second peak location was determined as 2.887 Å, as a lattice parameter of the model alloy. This result is in good agreement with the experimental result of 2.88 Å [5]. The second peaks have not been shown clearly from the RDF curves because they shift toward the right side of the first peaks and make them expand. The atomic vibrations decrease as the temperature decreases and the bcc peak locations become clearer. As seen from the figure, when the temperature decreases to 400 K, the model system transforms to the martensite structure. Reverse transformation from martensite to austenite at 550 K has also been observed in heating process, as shown in Figure 2.

The atomic locations of the austenite and martensitic phases for the model alloy can be seen in Figure 3. Here,

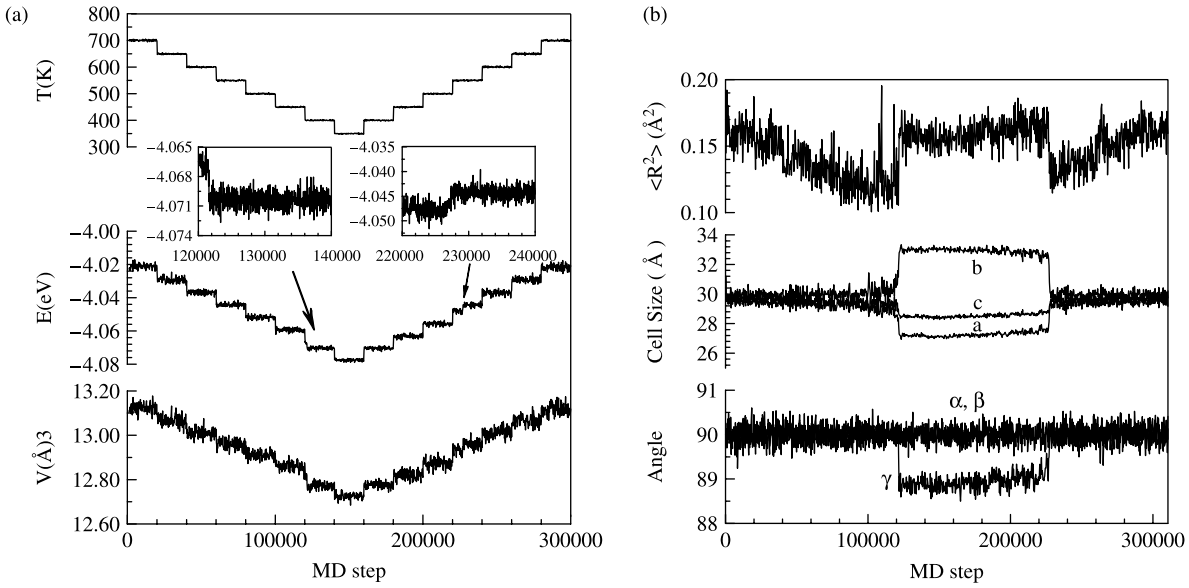

Figure 1. For the model system under zero pressure; (a) temperature, potential energy, volume (b) MSD, the lengths and angles of the MD cell axis.

the blue and red circles denote Ni and Al atoms, respectively. The sliding planes are shown by the arrows in Figure 3. In the proposal of Mao *et al.* [27], one set of parallel (110) planes in the original bcc structure becomes close-packed by contracting along the [001] direction, and sliding relative to one another in the $[\bar{1}10]$ and $[1\bar{1}0]$ directions so that neighbouring planes fit together. Experimental studies reveal that the B2-type martensite structures have the layered structures which consist of an array of close-packed planes [28].

The layered structures are characterised by the stacking sequence depending on the order in parent austenite phase. The product martensite in β-phase alloys has an internally faulted complex structure which has a long period stacking order, such as the 9R or 18R type structure [29]. Nevertheless, the stacking sequences have not been clearly obtained in the present model system, because of the insufficient number of atoms employed in the simulations. Although our model alloy has the stacking sequence structure in martensite phase, we cannot give a proper name to this layered structure such as 7R, 9R or 18R, due to the constrained length of the MD cell axis. However, Schryvers [30] experimentally observed the 7R type stacking sequence in Ni–Al alloys, as we have theoretically obtained in recent research [3,31,32]. It can be said that the thermally induced austenite ↔ martensite phase transformations in Ni-37.5 at.%Al alloy system can be modelled successfully by the SCEAM based on the

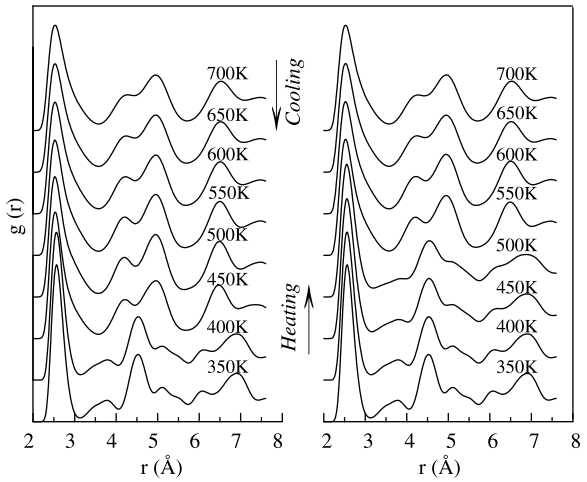

Figure 2. The curves of radial distribution functions at different temperatures during cooling and heating cycle.

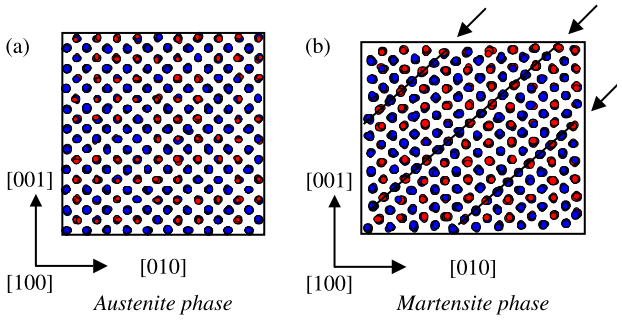

Figure 3. View of atomic location from [100] direction in (a) austenite and (b) martensite phases during thermal-induced martensitic transformation. Ni and Al atoms are denoted with blue and red circles.

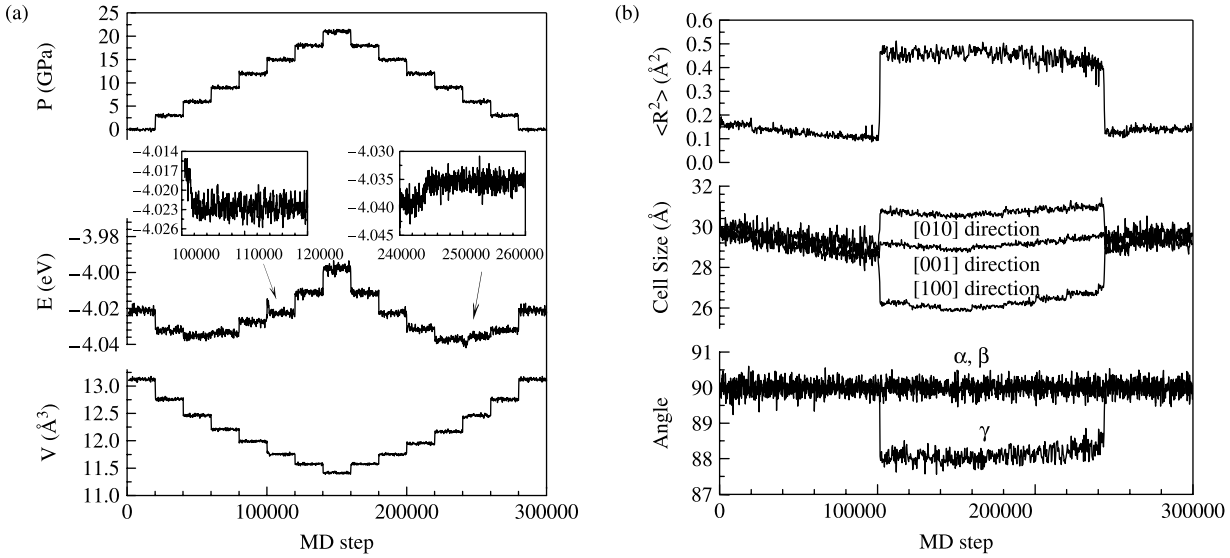

Figure 4. Changes of some quantity for the model system at 700 K constant temperature during pressure-induced transformation. (a) Applied pressure on the system, cohesive energy, volume. (b) MSD, lengths and angles of MD cell axis.

many-body idea, apart from our other study based on the pair interactions [3,33].

3.2 Pressure induced transformation

In order to observe pressure-induced transformation in our model system, we performed the programme of pressure change at 700 K constant temperature, as seen in Figure 4(a). In this programme the pressure acting on the system increases from zero to 21 GPa with intervals of 3 GPa and decreases with the same ratio. The simulations run for 20,000 integration steps at each pressure. It can be seen clearly from Figure 4(a) that, when the pressure reaches a value of 6 GPa a minimum value of the cohesive energy is obtained. The mean of decreasing in cohesive energy is that the system forms a more stable structure. When the pressure is raised to 15 GPa, the changes in the structural quantities such as MSD and the length of the MD cell axis (Figure 4(b)) appear. The deviation in the MSD after the transformation is calculated as 0.4 Å^2. It can be said that the pressure-induced transformation from the austenite to the martensite phase in the model system has a diffusionless character as with the thermally induced case. From Figure 4(b), the length of the MD cell axis is calculated as $\langle A\rangle = 26.26$ Å ([100] direction), $\langle B\rangle = 30.74$ Å ([010] direction), $\langle C\rangle = 29.13$ Å ([001] direction), taking the time average over the last 10,000 integration steps at 21 GPa pressure. From these values, it can be interpreted that the MD cell has a tetragonal distortion of $C/A = 1.11$ after the transformation.

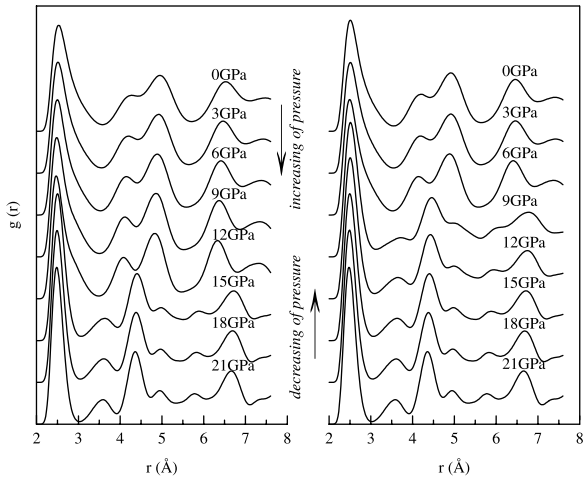

Figure 5. The curves of radial distribution functions at different pressures during increasing and decreasing pressure cycles.

RDF curves plotted as an average of time and particle numbers at different pressures are shown in Figure 5. With increasing pressure the intensities of the first peaks of RDF curves begin to rise before the transformation from the austenite to the martensite phase, because the coordination number of the martensite phase (with fcc unit cell of 12 coordination number) is higher then that of the austenite phase which has a bcc unit cell with eight coordination number. Also, before the transition, the first peak widths are narrowed by the efforts that the second-nearest neighbouring atoms become the nearest neighbouring. The stable structure of the model system in the austenite phase at 700 K is preserved until the pressure reaches a value of 15 GPa. However, the transformation from austenite to martensite

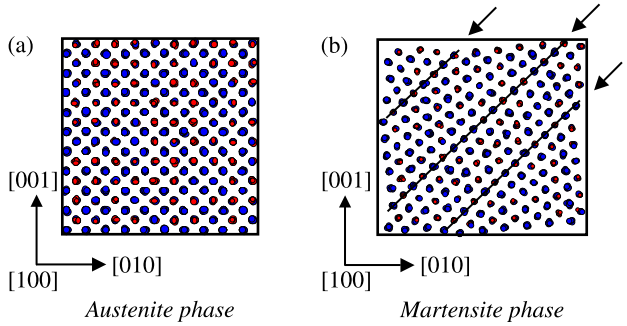

Figure 6. View of atomic location from (100) direction in (a) austenite and (b) martensite phases during pressure-induced martensitic transformation. Ni and Al atoms are denoted with blue and red circles.

begins at 15 GPa. It can been seen from the right side of Figure 5 that, in the reverse process with decreasing of pressure, the martensite structure is stable until 6 GPa. The reverse transformation is completed by conveying the applied pressure on the system to 6 GPa when the original austenite B2 structure occurs newly. After this, the model system in the austenite structure is stable until zero pressure. Upon unloading (decreasing pressure), the system completely recovers (pseudoelastic) at higher temperature [34].

The views of atomic locations in the martensitic structure after the reverse transformation is completed are shown in Figure 6. Ni and Al atoms are denoted with blue and red circles in the figure, respectively. The sliding planes are shown in Figure 6 by the arrows.

4. Conclusion

Both thermally and pressure-induced martensitic phase transformations for Ni-37.5 at.%Al model alloy system have been studied by using the anisotropic MD computer simulations. To model the alloy system the Sutton–Chen version of the EAM has been used with the original parameters, given in literature, for the monatomic interactions in the alloy. However, by using the parameters obtained from the mixing rule for the cross interactions, we could not observe the stable model system in β-phase of B2 type super-cell. Therefore, only the potential parameter was optimised by means of MD simulations and was estimated as 0.0201 eV. These observations make our study different from the others based on the pair potential energy functions. The pseudo-elasticity properties observed in the shape memory alloys have been observed during the process of increasing and decreasing pressure.

References

[1] D.A. Porter and K.E. Easterling, *Phase Transformations in Metals and Alloys*, 2nd ed., Chapman & Hall, T.J. Press (Padstow) Ltd., Cornwall, 1992.
[2] Z.G. Wang, X.T. Zu, and Y. Huo, *Effect of heating/cooling rate on the transformation temperatures in TiNiCu shape memory alloys*, Thermochim. Acta 436 (2005), p. 153.
[3] S. Kazanc, S. Ozgen, and O. Adiguzel, *Pressure effects on martensitic transformation under quenching process in a molecular dynamics model of NiAl alloy*, Phys. B 334 (2003), p. 375.
[4] P.H. Kitabjian et al., *High-temperature deformation behaviour of NiAl(Ti) solid–solution single crystals*, Metall. Mater. Trans. A 30A (1999), p. 587.
[5] D.B. Miracle, *The physical and mechanical properties of NiAl*, Acta Metall. Mater. 41(3) (1993), p. 649.
[6] R.J. Comstock et al., *Modeling the transformation stress of constrained shape memory alloys single crystals*, Acta Mater. 44(9) (1996), p. 3505.
[7] A. Chrysochoos, H. Pham, and O. Maisonneuve, *Energy balance of thermoelastic martensite transformation under stress*, Nuclear Eng. Des. 162 (1996), p. 1.
[8] Z.K. Lu and J. Weng, *A self-consistent model for the stress-strain behaviour of shape-memory alloy polycrystals*, Acta Mater. 46(15) (1998), p. 5423.
[9] J.M. Haile, *Molecular Dynamics Simulation, Elementary Methods*, Wiley, Mississauga, 1992.
[10] R. Meyer and P. Entel, *Lattice dynamics of martensitic transformations examined by atomistic simulations*, J. Phys. IV Fr. 7ab 29 (1997), p. C5.
[11] Y. Shao, P.C. Clapp, and A. Rifkin, *Molecular dynamics simulation of martensitic transformations in NiAl*, Metall. Mater. Trans. A 27A (1996), p. 1477.
[12] E.S. Lee and S. Ahn, *Changes in features of invariant plane strain with monoclinic distortion in 18R-type martensitic transformation*, Acta Mater. 46(12) (1998), p. 4357.
[13] P. Dang and M. Grujicic, *The effect of crack-tip material evolution on fracture toughness an atomistic simulation study of the Ti–V alloy system*, Acta Mater. 45(1) (1997), p. 75.
[14] X. Ding et al., *Precursors to stress-induced martensitic transformations and associated superelasticity: molecular dynamics simulations and an analytical theory*, Phys. Rev. B 74 (2006), p. 104,111.
[15] H.S. Park and V. Laohom, *Surface composition effects on martensitic phase transformations in nickel aluminium nanowires*, Philos. Mag. 87 (2007), p. 2159.
[16] H.S. Park, *Stress-induced martensitic phase transformation in intermetallic nickel aluminum nanowires*, Nano Lett. 6 (2006), p. 958.
[17] A.F. Voter and P. Chen, *Accurate interatomic potentials for Ni, Al and Ni_3Al*, Mat. Res. Soc. Symp. Proc. Materials Research Society 82 (1987), p. 175.
[18] M.W. Finnis and E. Sinclair, *A simple empirical N-body potential for transition metals*, Philos. Mag. A 50(1) (1984), p. 45.
[19] A.P. Sutton and J. Chen, *Long-range Finnis–Sinclair potentials*, Philos. Mag. Lett. 61 (1990), p. 139.
[20] T. Çağın et al., *Thermal and mechanical properties of some fcc transition metals*, Phys. Rev. B 59(5) (1999), p. 3468.
[21] R.A. Johnson, *Alloy models with the embedded-atom method*, Phys. Rev. B 39(17) (1989), p. 12554.
[22] M. Parrinello and A. Rahman, *Crystal structure and pair potentials: a molecular-dynamics study*, Phys. Rev. Lett. 45(11) (1980), p. 1196.
[23] J.M. Haile, *Molecular Dynamics Simulation, Elementary Methods*, John Wiley & Sons, Inc., Mississauga, 1992.

[24] D.W. Heermann, *Computer Simulation Methods in Theoretical Physics*, Springer-Verlag, Berlin, 1986.
[25] M. Parrinello and A. Rahman, *Polymorphic transitions in single crystals: a new molecular dynamics method*, J. Appl. Phys. 52(12) (1981), p. 7182.
[26] Z. Nishiyama, *Martensitic Transformation*, Academic Press, New York, NY, 1978.
[27] H. Mao, W.A. Bassett, and T. Taskahashi, *Effect of pressure on crystal structure and lattice parameters of iron up to 300 kbar*, J. Appl. Phys. 38 (1967), p. 272.
[28] K.Y. Lee and R. Ray, *Mechanism of pressure-induced martensitic phase transformations: a molecular-dynamics study*, Phys. Rev. B 39(1) (1989), p. 565.
[29] W.R. Dong et al., *Effects of ordering type and degree on monoclinic distortion on 18R-type martensite in Cu–Zn–Al Alloys*, Metall. Trans. A 23A (1992), p. 2753.
[30] D. Schryvers, *Nucleation and growth of the Ni_5Al_3 phase in Ni–Al austenite and martensite*, J. Phys. IV 5(C2) (1995), p. 225.
[31] S. Ozgen and O. Adiguzel, *Investigation of the thermoelastic phase transformation in a NiAl alloy by molecular dynamics simulation*, J. Phys. Chem. Solids 65(5) (2004), p. 861.
[32] S. Kazanc, S. Ozgen, and O. Adıguzel, *The role of hydrostatic pressure on the characteristics of thermoelastic phase transformation: a molecular dynamics simulation*, Balkan Physic Lett. 12(2) (2004), p. 98.
[33] S. Ozgen and O. Adiguzel, *Molecular dynamics simulation of diffusionless phase transformation in a quenched NiAl alloy model*, J. Phys. Chem. Solids 64 (2003), p. 459.
[34] Y.Y. Ye et al., *Pseudoelastic behaviour of hypostoichiometric NiAl alloys: a simple model*, Phys. Rev. B 49(9) (1994), p. 5852.